Inorganic Chemistry

Forum Article

pubs.acs.org/IC

Homolytic N−H Activation of Ammonia: Hydrogen Transfer of Parent Iridium Ammine, Amide, Imide, and Nitride Species

Markus G. Scheibel,[†] Josh Abbenseth,[†] Markus Kinauer,[†] Frank W. Heinemann,[∥] Christian Würtele,[†] Bas de Bruin,*[,‡] and Sven Schneider*[,†]

[†]Institut für Anorganische Chemie, Georg-August-Universität, Tammannstraße 4, 37077 Göttingen, Germany

[∥]Department of Chemistry and Pharmacy, Inorganic Chemistry, Friedrich-Alexander University Erlangen−Nürnberg (FAU), Egerlandstr. 1, 91058 Erlangen, Germany

[‡]Homogeneous and Supramolecular Catalysis group, van 't Hoff Institute for Molecular Sciences (HIMS), University of Amsterdam, 1090 GD Amsterdam, The Netherlands

Supporting Information

ABSTRACT: The redox series $[Ir^{n}(NH_x)(PNP)]$ (n = II−IV, x = 3−0; PNP = N(CHCHPtBu$_2$)$_2$) was examined with respect to electron, proton, and hydrogen atom transfer steps. The experimental and computational results suggest that the Ir^{III} imido species $[Ir(NH)(PNP)]$ is not stable but undergoes disproportionation to the respective Ir^{II} amido and Ir^{IV} nitrido species. N−H bond strengths are estimated upon reaction with hydrogen atom transfer reagents to rationalize this observation and are used to discuss the reactivity of these compounds toward E−H bond activation.

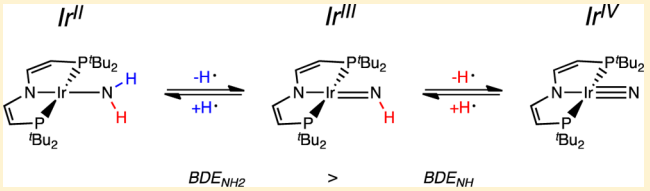

1. INTRODUCTION

The chemistry of transition metal (TM) complexes with covalently bound nitrogen ligands, i.e. amido, imido, and nitrido species $L_nM{-}NR_x$, has undergone a renaissance in recent years due to their relevance to catalytic transformations.[1] For example, efficient nitrene (N−R) transfer protocols, such as C−H amination (Scheme 1) or olefin aziridination, rely on TM catalysts,[2] particularly with late, electron rich transition metals, like rhodium and copper. At the current point of mechanistic understanding, the nitrenoid character of reactive $L_nM{-}NR$ intermediates determines their reactivity relevant to catalysis. The electronic structures of these transient species and the precise mechanistic pathways of nitrene transfer are subjects of current experimental and computational studies. However, some general features of late TM bonding to strong π-donors like imido and nitride ligands provide qualitative rationalization. Decreasing valence d-orbital energies along the transition series[3] suggests more and more covalent metal nitrogen bonding. Furthermore, rising d-orbital occupancy can lead to destabilizing repulsive M(d)−N(p) filled−filled interactions for late transition metal ions. These trends parallel several experimental findings:

−The bond energies of the diatomic gas phase species $[M{\equiv}N]^+$ decrease from Ti to Cu.[4] This observation is also reflected in the scarcity of terminal imido and particularly nitrido complexes of TMs beyond group 8 (see below).

−While early TM complexes typically exhibit distinct nucleophilic imide or nitride ligand reactivity, late TM examples often show increased electrophilic (or ambiphilic) nitrogen reactivity. Within a simple molecular orbital (MO) picture, the higher degree of covalency translates into an increasing N(p) orbital contribution to the M−N π* MOs. These often define the LUMO of closed-shell imido or nitrido complexes, providing a rationale for increasing N electrophilicity (or ambiphilicity) for such compounds.

−In turn, species that result from their (formal) reduction, i.e. with populated M−N π* antibonding levels, exhibit reduced

Scheme 1. Generation and Transfer of Nitrene Species via Two- (red) and One-Electron (blue) Oxidation Pathways

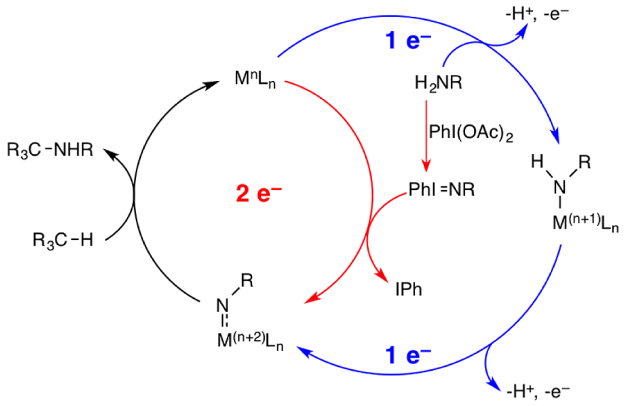

Special Issue: Small Molecule Activation: From Biological Principles to Energy Applications

Received: April 12, 2015
Published: July 20, 2015

DOI: 10.1021/acs.inorgchem.5b00829
Inorg. Chem. 2015, 54, 9290−9302

M−N bond order and increased nucleophilic (or ambiphilic) *N* reactivity. Furthermore, ligand centered radical reactivity might be attributed to delocalization of spin density on the nitrogen ligand.

Similar considerations as for nitrene reactivity apply to nitrene generation. Such species are generally obtained from reaction with preoxidized nitrogen sources, such as organic azides or iminoiodinane reagents from in situ oxidation of amines with hypervalent iodine oxididant. Hence, C−H amination usually follows a two-electron nitrene generation and transfer cycle (Scheme 1).[5] Warren and co-workers reported copper catalyzed amination of benzylic substrates, directly using primary and secondary amine nitrogen sources and di-*tert*-butylperoxide as an oxidant.[6] The authors showed that a copper(II) intermediate with amido ligand radical character undergoes HAA from the hydrocarbon substrate. In analogy, a two-step, one-electron redox regime was proposed by Berry and Kornecki for dirhodium catalyzed nitrene transfer with amine and cerium(IV) as oxidants, as sketched in Scheme 1 (blue cycle).[7] This approach might be promising with respect to the direct employment of amines, or even ammonia, as substrates in C−H amination. It could also afford the use of more sustainable chemical oxidants or electrocatalytic amination. Furthermore, besides *partial* amine oxidation, *full* oxidation of ammonia to dinitrogen represents the anodic half-reaction in direct ammonia fuel cells (DAFC), which are under investigation in the context of nitrogen based energy storage schemes.[8] In turn, the reverse reaction, i.e. electrochemical nitrogen fixation, is a highly desirable goal for electrocatalysis.[9]

Despite this general interest in amine, especially ammonia oxidation, it is far from having been broadly examined. As for parent ammonia, both the high bond dissociation enthalpy (BDE_{N-H}: 104 kcal mol^{-1})[10,11] and the low acidity (pK_a^{dmso} = ~41)[12] render activation at mild conditions a challenging task. Redox-neutral N−H heterolysis of ammonia is observed upon protonolysis of basic ligands, e.g. hydrides or alkyls (Scheme 2a), upon 1,2-addition across metal−ligand multiple bonds (e.g., M=CR_2), or upon proton transfer to other basic groups in the first or second coordination sphere ("metal−ligand cooperative activation," Scheme 2b).[13] In contrast, ammonia oxidative addition to a single (Scheme 2c) or two metal centers (Scheme 2d) is rare;[14,15] homolytic activation upon HAA from TM coordinated NH_3 (Scheme 2e) was not reported.

Scheme 2. Transition Metal Mediated Ammonia Activation

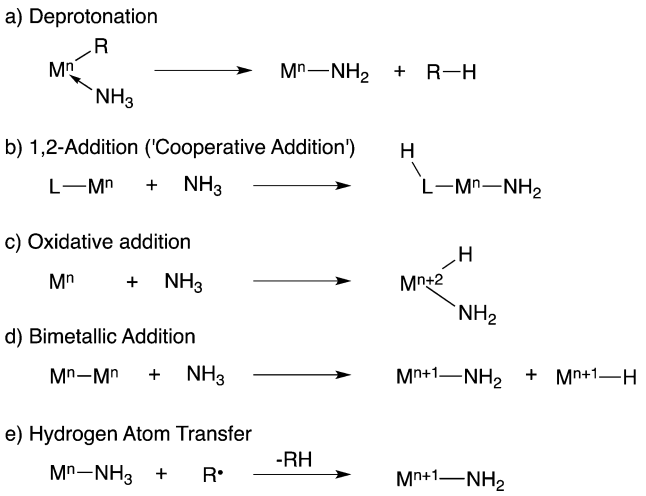

In this forum article, we first want to discuss the previously reported reactivity of TM imido and nitride complexes beyond group 8, which is relevant to catalytic transformations like nitrene transfer. Some comprehensive, excellent reviews on imide/nitride chemistry were published in recent years.[1] Therefore, we do not intend to give an exhaustive summary. Instead, we want to emphasize the role of open-shell species with partial nitrogen ligand radical character with the help of experimentally well-defined examples. In the main body of this paper, we then describe an experimental and computational study of a novel iridium(II−IV) parent amido, imido, and nitrido redox series and discuss the thermochemistry of hydrogen transfer in the context of ammonia activation.

1.1. Imido Complexes. Within group 9, pseudotetrahedral M^{III} (M = Co, Rh, Ir) imidos are best characterized and were reported from the groups of Bergman, Peters, Meyer, Theopold, Smith, and Tejel (Figure 1).[16] Notably, complex **E** was not prepared with an azide precursor but from the respective cobalt(II) amido complex upon HAA with the 2,4,6-tri-*tert*-butylphenoxy radical. This reaction is consistent with a computed N−H bond dissociation enthalpy in the amido complex of 75 kcal mol^{-1}.[16g] Hence, HAA from an unactivated hydrocarbon will be thermochemically unfavorable. Complexes **A**−**F** exhibit two-electron, electrophilic imido group reactivity, such as NR transfer to phosphines, CO, or isocyanate, as expected from their low-spin (S = 0) ground states. Interestingly, Theopold et al. (Figure 1, **F**) and Betley et al. (Scheme 3) reported Co imido complexes with thermally accessible open-shell states.[16e,f,17] In fact, these compounds also undergo radical-type nitrene group transfer upon intramolecular insertion into benzylic C−H bonds (Scheme 3).

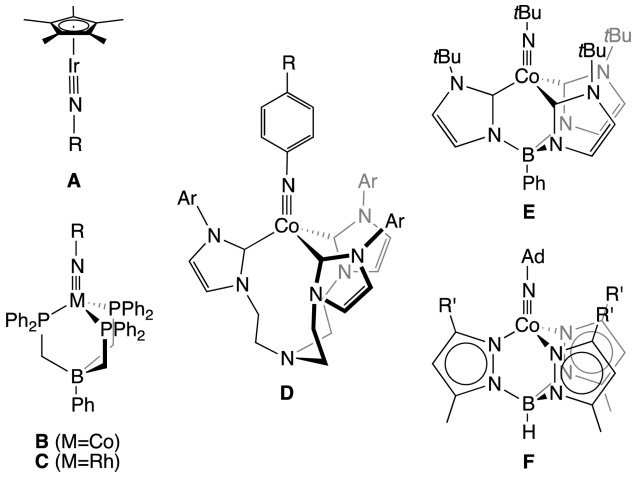

Figure 1. Pseudotetrahedral group 9 imido complexes with low-spin ground states.[16]

Scheme 3. Intramolecular C−H Amination Reported by Betley and Co-workers[17]

DOI: 10.1021/acs.inorgchem.5b00829
Inorg. Chem. 2015, 54, 9290−9302

Scheme 4. (Top) Proposed Mechanisms for C−H Amination and Aziridination Catalyzed by Cobalt(II) Porphyrin Complexes and (Below) Formation of Spectroscopically Characterited Key Intermediates G and H (Ligand L Currently Remains Unclear, but Is Likely an Amine or Amido Donor)[18]

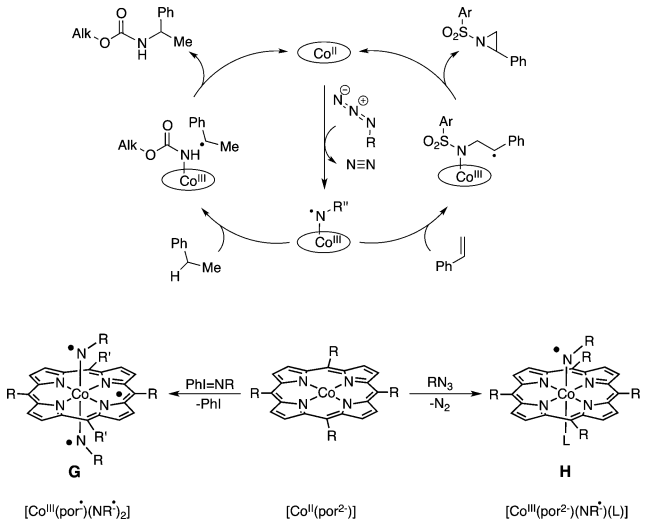

The groups of De Bruin and Zhang exploited imido radical reactivity for C−H bond amination and olefin aziridination catalyzed by cobalt porphyrin complexes (Scheme 4).[18] The nitrene-radical character for the key intermediates formed with organic azides (mononitrene **H**) and iminoiodinanes (bisnitrene **G**), respectively, was most recently demonstrated spectroscopically.[18g]

The three-coordinate, closed-shell nickel complexes with chelating bisphosphine and bis-NHC-carbene of type **I** (Scheme 5) that were established by Hillhouse et al. represent

Scheme 5. HAA Reactivity and Aryl Coupling of Nickel(III) Imido Radical Complexes (Ad = 1-Adamantyl)

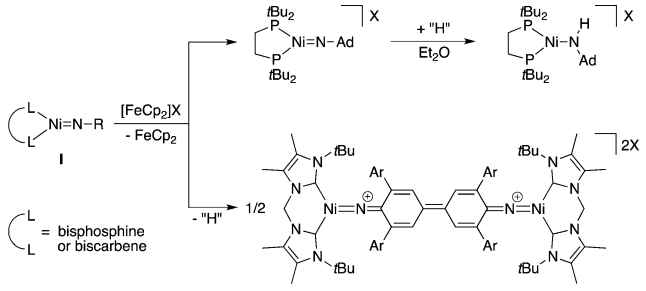

a key system in the exploration of late transition metal imido chemistry.[19] Notably, the Ni−N−R angles were found to vary from linear (180°) to strongly bent (127°). Detailed bond analysis revealed a reduced Ni−N bond order, i.e. considerably smaller than three also for virtually linear examples, which is expressed in distinctly nucleophilic imide reactivity, e.g. upon [2 + 2] cycloaddition with aldehydes or heterocumulenes.[20] Hence, oxidation to $[L_2Ni(NR)]^+$ should result in ligand centered radicals, which is in fact supported by DFT and reactivity:[21] Reaction of [(diphosphine)Ni(NAd)] with ferrocenium results in HAA even from diethyl ether to give nickel(II) amido complexes (Scheme 5). Alternatively, aryl C−C coupling was found for a dicarbene arylimido analogue (Scheme 5), attributable to spin-delocalization into the aromatic moiety.[22] This reactivity was previously reported, e.g. for dirhodium and nickel aryl imido complexes by Sharp et al. and Stephan and Bai, respectively.[23]

The HAA reaction of transient $[(\text{diphosphine})Ni^{III}(NAd)]^+$ with weak hydrogen donors like diethyl ether contrasts with the stability of $[(\text{diphosphine})Ni^{II}(NAd)]$, e.g. in THF. In fact, the nickel(II) arylimides can be prepared by HAA of the respective Ni^I amide with the 2,4,6-tri-*tert*-butylphenoxyl radical.[19c,20b] This allows for an estimate of the upper limit of BDE_{N-H} in the nickel(I) anilides of around 82 kcal mol^{-1}. That value is around 10 kcal mol^{-1} smaller than BDE_{C-H} data of typical ethereal solvents,[24] which is in agreement with the absence of solvent radical activation by the nickel(II) imides. Albeit only qualitative in nature and omitting kinetic influences, this comparison between the nickel(II) and nickel(III) imides showcases how radical reactivity is promoted by one-electron redox steps leading to ligand radical character.

Warren and co-workers proposed redox noninnocent imido ligand character for $S = 1/2$ nickel complex **J** (Scheme 6),[25]

Scheme 6. Benzylic C−H Activation with Diketiminato Nickel(III) Imido Complexes[26]

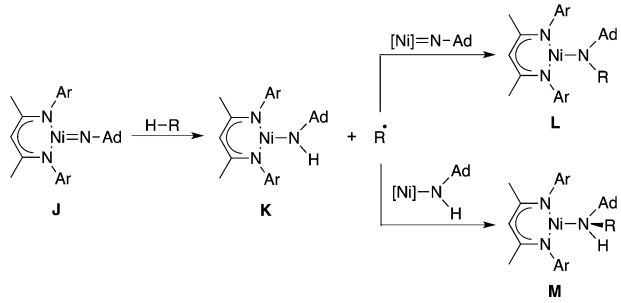

supported by large nitrogen hyperfine interaction detected by EPR and computational analysis. The ligand radical character is reflected in the HAA reactivity:[25,26] Amido complex **K** and benzene are obtained from the reaction with 1,4-cyclohexadiene. With benzylic hydrocarbon substrates, mixtures of amides **K** and **L** and the amine complex **M** are obtained, which was rationalized by HAA and subsequent competitive trapping of the hydrocarbyl radical.

Efficient, catalytic adamantyl nitrene C−H insertion was reported for an analogous diketiminato copper system by Warren and co-workers.[27] The respective terminal copper nitrene complex was proposed as a reactive intermediate but remains elusive. In an elegant study, Ray and co-workers demonstrated the stabilization of a transient copper nitrene complex by various Lewis acids (Scheme 7).[28] Characterization of the scandium adduct by XAS, UV−vis, and Raman spectroscopies afforded a detailed model of the (electronic) structure. Importantly, the Lewis acid adducts still undergo HAA reactivity and nitrene C−H insertion with hydrocarbons.

1.2. Nitrido Complexes. The chemistry of terminal transition metal nitrido complexes beyond group 8 is much less developed. Well-defined nitrides are restricted to group 9. The first example, iridium pyridinediimino (PDI) nitride **N**, was reported by Burger and co-workers in 2009 (Figure 2).[29] The electronic structure of diamagnetic **N** was described as $[(Ir^{III})(N^-)(PDI^{2-})]$. The resulting ambiphilic nitride character is expressed, e.g. by high basicity and the facile electrophilic

DOI: 10.1021/acs.inorgchem.5b00829
Inorg. Chem. 2015, 54, 9290−9302

Scheme 7. Lewis Acid Stabilization and HAA Reactivity of a Copper Nitrene Complex[28]

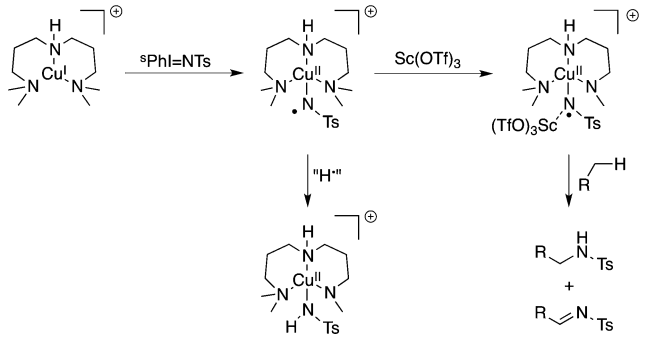

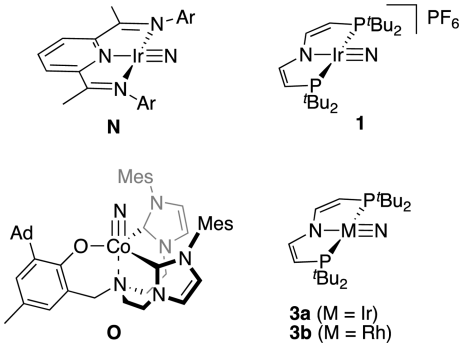

Figure 2. Characterized group 9 terminal nitrido complexes.

nitride insertion into H_2 and silane Si–H bonds through a concerted, two-electron mechanism.[29a,30]

Schneider and co-workers reported the isolation of electrophilic, closed-shell nitride $[Ir(N)(PNP)]PF_6$ (**1**; PNP = $N(CHCHP^tBu_2)_2$; Figure 2) upon oxidation of iridium(II) azide **2a** (Scheme 8).[31] One-electron reduction of closed-shell

Scheme 8. Formation of Iridium and Rhodium Nitrides and Coupling to N_2[31,32]

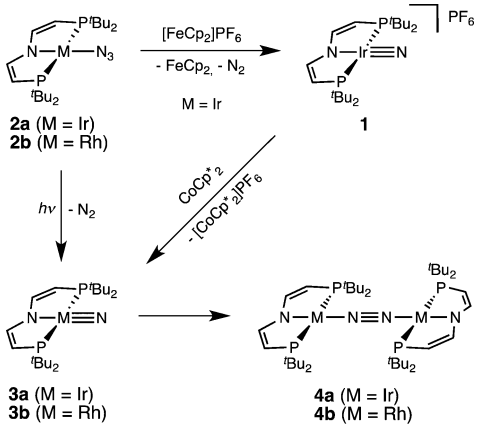

nitride **1** or irradiation of **2a** or the rhodium analogue, respectively, afforded the open-shell ($S = 1/2$) formally M^{IV} nitrides $[M(N)(PNP)]$ (M = Ir (**3a**), Rh (**3b**)).[31,32] Spectroscopic characterization indicated distinct π-radical (partial "nitridyl") character of the M–N fragment with M–N π^* antibonding character of the SOMO. The essentially equal distribution of excess spin over the metal and the nitride moiety underlines the strong covalency of iridium and rhodium nitride bonding. The transient nitrides undergo rapid, three-electron nitride coupling in solution toward bridging dinitrogen complexes $[(PNP)M(\mu^2{:}\eta_1{:}\eta_1\text{-}N_2)M(PNP)]$ (M = Ir (**4a**), Rh (**4b**)).

Meyer and co-workers recently reported the EPR spectroscopic characterization of a transient, terminal cobalt(IV) nitride in frozen solution (Figure 2, **O**).[33] According to the computational analysis, highly covalent M–N bonding was pointed out leading to considerable nitride ligand radical character, as in case of **3a**/**b**. In contrast to **3a**/**b**, this compound decays upon intramolecular nitride insertion into a Co–carbene bond.

De Bruin and Schneider also disclosed the synthesis and isolation of a nitrido bridged Rh^{II}/Rh^{III} complex using a sterically less protecting "pincer" ligand (Scheme 9, **P**).[34] Spectroscopic

Scheme 9. Proposed Mechanism for the Reaction of Bridging Nitride L with CO[34]

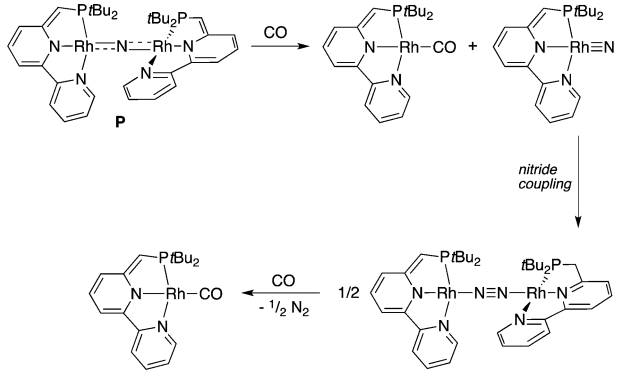

and computational analysis indicate an $S = 1/2$ ground state and spin delocalization over the Rh–N–Rh π-manifold with considerable spin density on the bridging nitrogen ligand. Reaction with CO yields the respective rhodium(I) carbonyl complex (Scheme 9). The proposed mechanism proceeds via dimer dissociation and nitride coupling of a transient, terminal rhodium(IV) nitride, as was directly observed for **3b**.

Nitride coupling to N_2 was also reported for several octahedral M^V group 8 nitrides,[35] and these low-spin complexes share an isolobal relationship with the square-planar M^{IV} group 9 nitrides (c.f. Discussion). In the context of nitrogen fixation, it is appealing to compare these with systems that undergo the microscopic reverse, i.e. N_2 splitting, through linear dinitrogen (or diazenido) complexes.

From simple qualitative orbital symmetry considerations, the {M–N–N–M} core in idealized rotational symmetry gives rise to a manifold of four degenerate pairs of π-MOs (Scheme 10).[36] The second lowest pair is M–N bonding and N–N antibonding in nature, while the next higher pair exhibits the opposite properties. The $\{M–N–N–M\}^8$ π-electron configuration features strong N_2 activation, as in the case of Bercaw's $[Cp_2^*(N_2)Zr(N_2)Zr(N_2)(Cp^*)_2]$.[37,38] However, the N–N σ^*-MO in the N_2-bridged complex drops upon N_2 splitting into nitrides (Scheme 10), which proceeds through a *zigzag* transition state. Therefore, the $\{M–N–N–M\}^8$ π-electron configuration is two electrons short to fill all bonding σ- and π-orbitals in the resulting nitrides upon N_2-splitting.[39] Hence, the $\{M–N–N–M\}^{10}$ π-configuration should be ideal to undergo N–N bond cleavage into stable nitrides.

In fact, these simple considerations apply to several systems in different coordination environments and molecular symmetries

DOI: 10.1021/acs.inorgchem.5b00829
Inorg. Chem. 2015, 54, 9290–9302

Scheme 10. Qualitative Orbital Interaction Diagram for N_2 Splitting/Coupling from/to a Linearly N_2-bridged Dinuclear Complex for the $\{M-N-N-M\}^{10}$ (blue) and the $\{M-N-N-M\}^{12}$ π Configurations (red) (adapted with permission from ref 39, copyright 1996 American Chemical Society)[a]

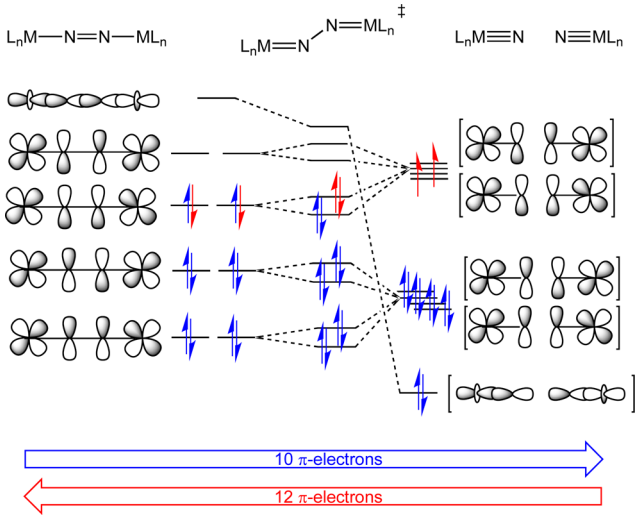

[a]Only the relevant M–N σ- and π-type orbitals are shown.

that were reported to split dinitrogen into terminal nitrides via linear μ^2:η_1:η_1-N_2 intermediates.[40] For example, each Mo ion in $(t\text{BuArN})_3\text{Mo}(N_2)\text{Mo}(N t\text{BuAr})_3$, which splits into nitrides, contributes three electrons to the π system, resulting in an overall $\{M-N-N-M\}^{10}$ π configuration.[39] In turn, the open-shell nitrides **3a**/**b** form dinitrogen-bridged complexes with square-planar coordinated M^I (M = Rh, Ir). Hence, the two filled orbitals with Ir–N π symmetry give rise to a $\{M-N-N-M\}^{12}$ configuration since each metal provides four π electrons. The same applies to the octahedral M^V (M = Fe–Os) nitrides that were shown to couple to N_2.[35] Another interesting example is provided by Peters' closed-shell iron(IV) nitride $[(BP_3)FeN]$ (BP_3^- = $PhB(CH_2PiPr_2)_3^-$), which couples to the N_2-bridged complex $[(BP_3)Fe(N_2)Fe(BP_3)]$.[41] There, the metal ions were described as high-spin Fe^I in C_{3v} symmetry resulting in a $(d_{xy},d_{x^2-y^2})^4(d_{z^2})^1(d_{xz},d_{yz})^2$ d-electron configuration. Hence, each iron atom contributes only two electrons to the π-manifold giving a $\{M-N-N-M\}^8$ π configuration in the dimer, which is in line with the overall thermochemistry that favors nitride coupling.

Although these electronic structure/reactivity considerations are very simplistic in nature, they provide some rationale for the underlying driving force of N_2 splitting and coupling. The relevant M–N bond strengths within these nitride vs dinitrogen complexes are certainly governed by many other contributions, which are beyond the scope of these rationalizations just based on orbital symmetry and occupation.

Interestingly, some terminal nitrides were directly demonstrated to undergo C–H amination or proposed as transient intermediates in HAA reactions toward amido or imido complexes.[42] Within group 9, Chirik observed intramolecular nitrogen insertion into a secondary C–H bond upon irradiation of a cobalt azide complex (Scheme 11).[43] In comparison, the generation of **3a**/**b** in the presence of H atom donors like 1,4-cyclohexadiene also resulted in nitride coupling, exclusively.

This striking preference of the open shell nitrides **3a**/**b** toward N_2 formation over HAA will be examined in the next

Scheme 11. Intramolecular C–H Amination upon Irradiation of a Cobalt Azide[43]

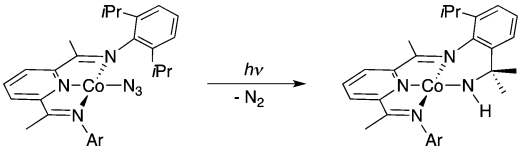

part of this paper. Within an experimental and computational study, we describe the reactivity of a redox series of iridium(II–IV) pincer complexes with parent ammine, amide, imide, and nitride ligands relevant to ammonia functionalization. Particular emphasis was put on estimating N–H BDEs of $M-NH_x$ species as they relate to the thermochemistry of HAT reactivity, such as radical C–H activation.

RESULTS

Syntheses. Salt metathesis of iridium(II) chloro complex $[IrCl(PNP)]$ (**5**)[44] with excess sodium amide in the presence of 15-crown-5 results in the selective formation of parent amido complex $[Ir(NH_2)(PNP)]$ **6** in over 60% isolated yield (Scheme 12). The magnetic moment of **6** (μ_{eff} = 1.82 μ_B,

Scheme 12. Syntheses of Iridium(II) and Iridium(III) Parent Amine and Amido Complexes

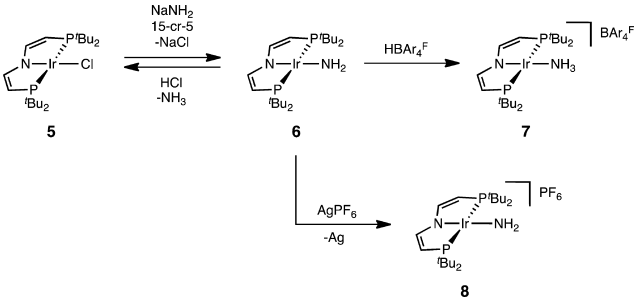

Evans' method) is in agreement with an S = 1/2 ground state. The X-band EPR spectrum (see Supporting Information) reveals a rhombic **g** tensor (g_x = 2.72, g_y = 2.12, g_z = 1.93) without resolved hyperfine interactions, characteristic for a metal dominated SOMO and predominant metal centered spin density (Ir, 68%; N, 27%; see Supporting Information). This observation contrasts with the formation of an aminyl radical complex upon oxidation of rhodium(I) amido complex $[Rh^I(trop_2N)(PR_3)]$.[45] The large **g** anisotropy of **6** is common for square planar d^7 complexes and is well reproduced by supporting DFT calculations (g_x = 2.69, g_y = 2.06, g_z = 1.96; see Supporting Information). The ^{1}H NMR spectrum of **6** exhibits three paramagnetically broadened and shifted signals for the pincer *t*Bu and CH groups, which is in agreement with the square-planar molecular structure obtained from X-ray diffraction (see below).

Protonolysis of **6** with HCl restores **5** quantitatively (Scheme 12). In contrast, the use of an acid with a weakly coordinating anion, $[H(OEt_2)_2][BAr_4^F]$ (BAr_4^F = $B(C_6H_3(CF_3)_2)_4$), allows for the isolation of the cationic iridium(II) ammine complex $[Ir(NH_3)(PNP)][BAr_4^F]$ (**7**). Single-crystals suitable for X-ray diffraction could be obtained as SbF_6-salt (see below). The X-band EPR spectrum of **7** (see Supporting Information) reveals an even more rhombic **g** tensor (g_x = 3.36, g_y = 1.82, g_z = 1.49) also without resolved hyperfine interactions. The **g** anisotropy is well reproduced by DFT calculations, which

DOI: 10.1021/acs.inorgchem.5b00829
Inorg. Chem. 2015, 54, 9290–9302

confirm predominant metal-radical (65%) character (see Supporting Information).

Chemical oxidation of **6** with $AgPF_6$ affords the isolation of the iridium(III) parent amido complex $[Ir(NH_2)(PNP)]PF_6$ (**8**) in 70% isolated yield (Scheme 12). In contrast to chloro complex $[IrCl(PNP)]PF_6$ (**9**), **8** is thermally stable at room temperature. X-ray single crystal diffraction (see below) confirms square-planar coordination of the metal ion, rendering complexes **8** and **9** the only known iridium(III) complexes in this geometry.[46] As reported for **9**, the sharp ^1H, ^{13}C, and ^{31}P NMR signals of **8** indicate a diamagnetic ($S = 0$) ground state and a C_{2v} symmetric molecular structure on the NMR time scale. The ^1H NMR signal assigned to the NH_2 group (δ = 11.35 ppm) exhibits a significant low-field shift compared with other parent iridium amido complexes (−1.3−6.0 ppm).[13i,14b,47] The diamagnetism of **8** and **9** contrasts with related d^6 complex [RuCl(PNP)], which adopts an intermediate-spin ($S = 1$) ground state,[48] attributed to larger ligand field splitting in case of the 5d ions and strong π-donation of the parent amido ligand (**8**), which destabilizes the LUMO.

In an attempt to synthesize parent iridium(III) imido complex [Ir(NH)(PNP)] (**10**), **8** was deprotonated with equimolar amounts of strong bases, such as $K[N(SiMe_3)_2]$ and KO*t*Bu (Scheme 13). Rapid and full conversion of the starting material

Scheme 13. Deprotonation of Complex 8 at Room Temperature

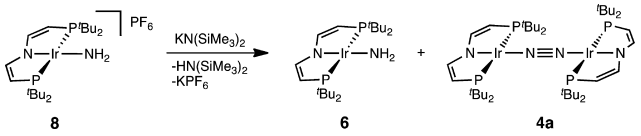

at room temperature was accompanied by selective formation of iridium(II) amide **6** (^1H NMR yield: 66%), the dinitrogen complex **4a** (33% including traces of $[Ir(N_2)(PNP)]$ (**11**)), and $H[N(SiMe_3)_2]$ (Supporting Information, Figure S3).[49] The reaction was monitored at −60 °C by NMR spectroscopy. At this temperature, the ^1H NMR spectrum revealed slow consumption of $K[N(SiMe_3)_2]$ toward $H[N(SiMe_3)_2]$ (Figure 3).

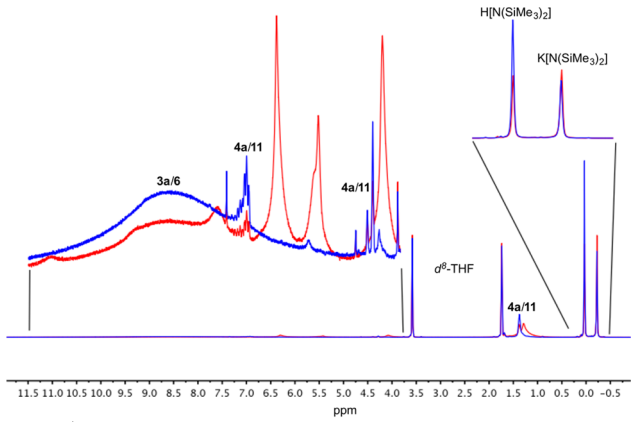

Figure 3. ^1H NMR spectra (d_8-THF, −60 °C) of the reaction of **8** with $K[N(SiMe_3)_2]$ directly after mixing (red line) and after shortly warming to room temperature (blue line), respectively.

The signals of diamagnetic starting material **8** immediately vanish despite only partial (ca. 50%) conversion of the base at this stage. However, equimolar mixtures of **8** with the final iridium(II) product **6** coalesce into extremely broad peaks at −60 °C due to self-exchange as shown with an original sample (see Supporting Information, Figure S4). Hence, full conversion of **8** cannot be assured despite the immediate absence of its NMR signals in this reaction. Importantly, four new peaks are observed at 1.24, 4.03, 5.42, and 6.27 ppm in about a 36:2:1:2 ratio of intensities, which cannot be assigned to **8** (Figure 3). At −60 °C, this intermediate is rapidly formed in high concentrations and vanishes upon shortly warming the sample to room temperature. Despite some peak broadening, the chemical shifts suggest diamagnetism for this intermediate. Hence, the peak intensities and shapes support the tentative assignment to diamagnetic imido complex **10** as a reactive intermediate, which rapidly decays even at low temperatures.

Molecular Structures. The molecular structures of **6**−**8** in the solid state were derived by single crystal X-ray diffraction (Figure 4), confirming square-planar coordination of the Ir ions

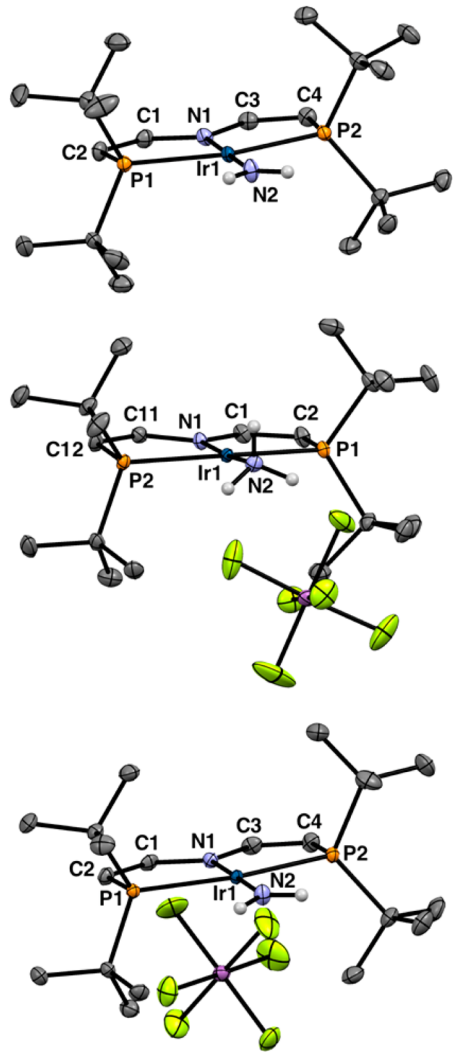

Figure 4. Molecular structures of **6** (top), **7** (center), and **8** (bottom) from X-ray diffraction with thermal ellipsoids at the 50% probability level (carbon bound hydrogen atoms and one molecule of THF in **7** are omitted for clarity).

in all cases. The structural features within the PNP pincer backbones of iridium(II) complexes **6** and **7**, such as C−N and C−C bond lengths (Table 1), strongly resemble those of the

DOI: 10.1021/acs.inorgchem.5b00829
Inorg. Chem. 2015, 54, 9290−9302

Table 1. Selected Bond Lengths and Angles of Amido Complexes 6 and 8 (x = 2) and Ammine Complex 7 (x = 3)

	6	7	8
	bond lengths [Å]		
Ir−N_{PNP}	2.0194(15)	1.9685(14)	1.926(2)
Ir−NH_x	1.9521(17)	2.1100(14)	1.900(2)
N−C	1.380(2)	1.391(2)	1.409(3)
	1.385(2)	1.392(2)	1.416(3)
C−C	1.348(3)	1.344(2)	1.331(4)
	1.344(3)	1.343(2)	1.329(4)
	bond angles [deg]		
N−Ir−N	179.74(7)	175.68(6)	179.07(10)
P−Ir−P	164.445(17)	165.703(15)	166.42(2)

chloro analogue **5**. Similarly, oxidation to iridium(III) exhibits the same trends for **8** and chloro complex **9**, i.e. shortening of Ir−N and C−C bonds and lengthening of C−N bonds. This trend indicates increased N to Ir π-donation upon oxidation of iridium(II) (S = 1/2) to iridium(III) (S = 0) as a result of the π^*-antibonding character of the SOMO (see Supporting Information). The Ir−NH_2 distance of **6** (1.9521(17) Å) compares well with other parent iridium amido complexes with a nitrogen donor ligand in the *trans* position (1.92−1.95 Å)[29] and is significantly shorter than examples with C-donor ligands trans to amide (2.00−2.19 Å).[14,47,50] The Ir^{n+}−NH_x distance decreases within the series **7** (x = 3, n = 2), **6** (x = 2, n = 2), and **8** (x = 2, n = 3) by more than 0.2 Å due to increasingly covalent σ- and π-bonding with the metal ion, resulting in a particularly short bond for **8** (1.900(2) Å). In comparison, the Ir−N triple bond length of $[Ir(N)(PNP)]^+$ (**1**) was reported to be at 1.678(4) Å.[31]

Electrochemical Examination. In analogy to **5**,[51] the cyclic voltammogram (CV) of **6** in THF (Figure 5) exhibits a reversible oxidation wave at $E_{1/2}$ = −0.68 V (vs Fc/Fc^+), which is in agreement with the isolation of oxidation product **8** (see above). Compared with Ir^{II}/Ir^{III} chloro complexes **5**/**9**, the potential ($E_{1/2}$) of the parent amido Ir^{II}/Ir^{III} redox couple **6**/**8** is shifted to lower potential by about 0.7 V, as a result of the increased amide vs chloride donor properties. Remarkably, the Ir^{IV}/Ir^{V} nitrido $[Ir(N)(PNP)]^{0/+}$ redox couple (**3a**/**1**) was found at a similar potential ($E_{1/2}$ = −0.86 V in THF, Supporting Information Figure S6) to that of **6**/**8**. This observation is in agreement with the high degree of covalency within Ir−NH_x (x = 0−2) bonding, as previously inferred for nitride **3a** from the EPR and ENDOR spectroscopic features.[31] Unlike for iridium(II) chloride **5**, electrochemical reduction of amide **6** in THF was found to be irreversible at all scan rates.

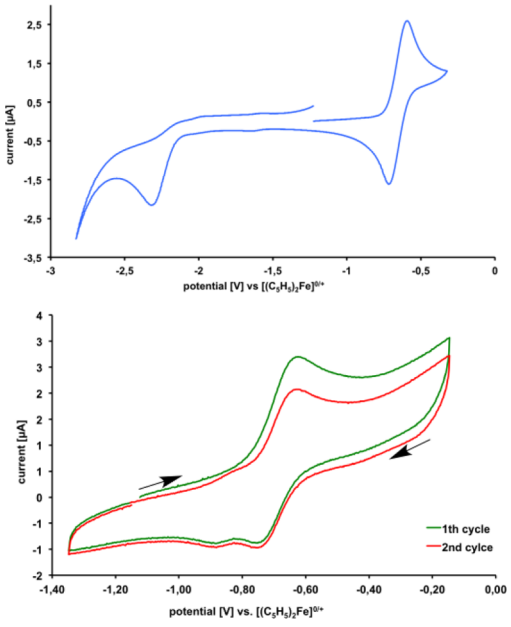

Figure 5. Top: CV of **6** (10^{-3} mol/L) in THF (400 mV/s, $[nBu_4N]PF_6$ 0.1 mol/L, Pt working, counter, and pseudo-reference electrodes). Bottom: CV of **6** (10^{-4} mol L^{-1}) in the presence of $K[N(SiMe_3)_2]$ (10^{-3} mol L^{-1}) in THF (800 mV s^{-1}, 0.1 mol L^{-1} $(nBu_4N)PF_6$, Pt working electrode and counter electrodes, Ag/Ag^+ reference electrode, potentials vs. $FeCp_2/FeCp_2^+$).

In contrast to the neutral conditions, the cyclic voltammogram of **6** in the presence of $K[N(SiMe_3)_2]$ (10 equiv) reveals increasingly irreversible oxidation at a high relative base concentration (Figures 5 and S5).[52] Furthermore, an additional reduction wave at $E_{1/2}$ = −0.86 V is observed upon cycling back after oxidation of **6**, which seems reversible at high scan rates. On the basis of the peak potential, this redox event is assigned to the $[Ir(PNP)(N)]^{0/+}$ (**3a**/**1**) redox couple (see above). Unfortunately, quantification of the currents that arise from the **6**/**8** and **3a**/**1** redox couples, respectively, is obscured by strong peak overlap, hampering quantitative kinetic analysis.

Reactivity of [Ir(NH_x)(PNP)] toward HAA. HAA within the $[Ir(NH_x)(PNP)]$ (x = 2−0) redox series was examined upon reaction of **6** (x = 2) with hydrogen atom acceptors and of **3a** (x = 0) with hydrogen atom donors, respectively (Scheme 14).[53] No reaction is observed upon the addition of TEMPO (2 eq.; TEMPO = 1-hydroxy-2,2,6,6-tetramethylpiperidine-1-yloxidanyl) to a solution of **6** in d_6-benzene (Scheme 14, reaction A; Supporting Information Figure S8). In reverse, the addition of 10 equiv of TEMPO-H (BDE_{O-H}(benzene) = 70 kcal mol^{-1})[54] to nitridyl complex **3a**, generated *in situ* by azide photolysis at −60 °C in d_8-toluene, leads to immediate formation of amide **6** (Scheme 14, reaction B; Supporting Information Figure S9).

An upper limit for the N−H BDEs was estimated upon reaction with 2,4,6-tri-*tert*-butylphenol (TBP-H; BDE_{O-H}(benzene) = 82 kcal mol^{-1})[54] and the 2,4,6-tri-*tert*-butylphenoxy radical (TBP), respectively. Photochemically generated **3a** (−60 °C, d_8-toluene) does not react with TBP−H (Scheme 14, reaction C; Supporting Information Figure S10). In contrast, **6** is immediately consumed in the presence of 2 equiv of TBP (reaction D, Supporting Information Figure S11), yet not as clean. Besides **3a**, considerable amounts of dinitrogen complex **4a** are also observed. The mechanism for the formation of **4a** remains unclear, as binuclear nitridyl coupling of **3a** is slower at −60 °C than the here observed formation of **4a**.[31] However, the generation of **3a** suggests that the absence of HAA from TBP−H by **3a** (Scheme 14, reaction C) can be attributed to the overall reaction thermochemistry rather than kinetics. Importantly, the reaction of **6** with only 1 equiv of TBP results in a mixture of approximately equimolar amounts of **3a** and **6** besides **4a** (Scheme 14, reaction E; Supporting Information Figure S12).

Assuming that imido complex $[Ir(NH)(PNP)]$ (**10**) is an intermediate in the HAT reactions with amide **6** and nitride **3a**, and that HAT is rapid under the experimental conditions, the following thermochemical estimates are made from the H-transfer experiments described above (Scheme 15):

$$BDE_{NH_2} \gtrsim 70 \text{ kcal mol}^{-1} \qquad \text{(reaction A)}$$

DOI: 10.1021/acs.inorgchem.5b00829
Inorg. Chem. 2015, 54, 9290−9302

Scheme 14. Reactions of Amide 6 and Nitride 3a with HAT Reagents

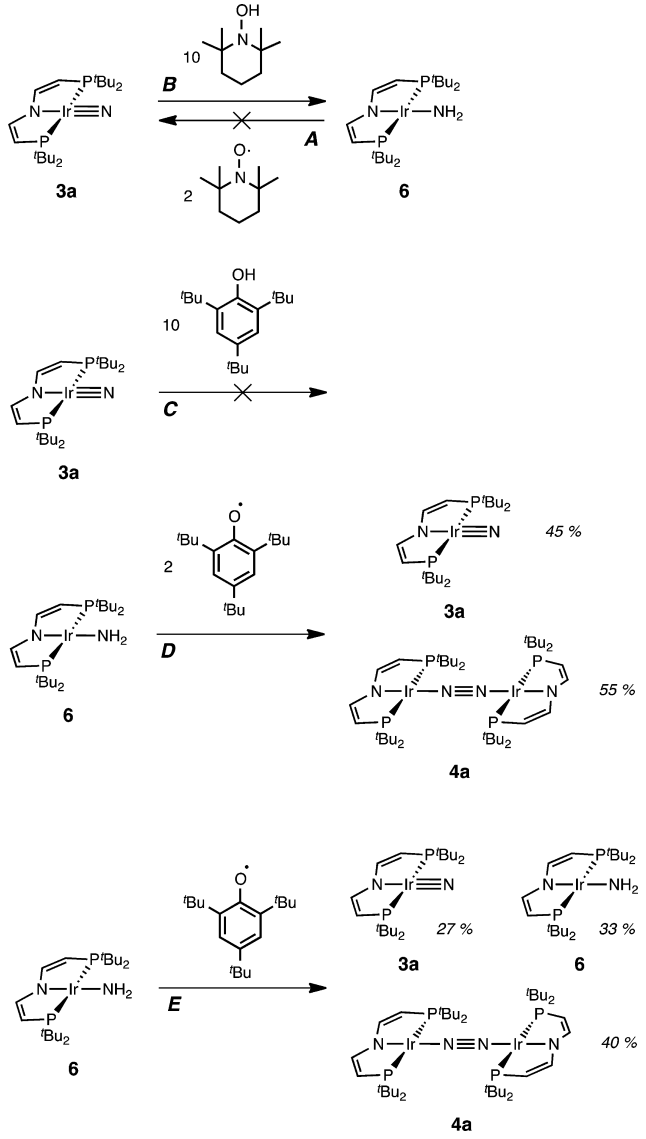

Scheme 15. HAT Reactions from Amide 6 to Nitride 3a via Proposed Imide Intermediate 10

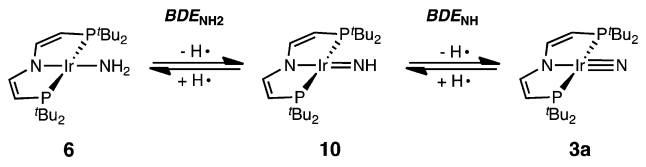

$$BDE_{NH} + BDE_{NH_2} \gtrsim 140 \text{ kcal mol}^{-1} \quad \text{(reaction B)}$$

$$BDE_{NH} \lesssim 82 \text{ kcal mol}^{-1} \quad \text{(reactions C and D)}$$

$$BDE_{NH} < BDE_{NH_2} \quad \text{(reaction E)}$$

Computational Examination. The N−H BDEs were also computationally evaluated with density functional theory (DFT). As previously reported for nitride **3a**,[31] the computed EPR features and molecular structure of amide **6** (S =1/2) are in excellent agreement with experimental results. However, assigning an electronic ground state structure and energy to postulated imido species **10** is much less straightforward. DFT geometry optimizations of **10** in triplet (T), open shell singlet (OSS), and closed shell singlet (CSS) states place all three configurations within around 1 kcal mol^{-1} (see Supporting Information). The OSS configuration turned out to be the most stable, which would in fact be in agreement with the tentative assignment of NMR signals to **10** (see above). In the triplet state, the Ir−N−H angle (142.0°) is considerably closer to linearity as compared with the CSS (114.2°) and OSS (117.1°) states, respectively, resulting in two energetically almost degenerate SOMOs with strong d(Ir)−p(N) π^* character for the triplet (see Supporting Information). Ir−N−H bending reduces this interaction for one of the two orbitals and stabilization of the singlet states. However, in all cases Ir−NH bonding is comprised of six electrons in orbitals with σ- (2e$^-$) and π-type (4e$^-$) symmetry and two electrons in π^* orbitals with strongly covalent bonding to the metal ion resulting in low-lying open-shell states (see Supporting Information for further discussion).

$$[Ir(NH_2)(PNP)] \rightarrow [Ir(NH)(PNP)] + H^{\bullet}$$
$$\Delta H_r \cong +95 \text{ kcal mol}^{-1} \quad (BDE_{NH_2}) \qquad (1)$$

$$[Ir(NH)(PNP)] \rightarrow [Ir(NH)(PNP)] + H^{\bullet}$$
$$\Delta H_r \cong +71 \text{ kcal mol}^{-1} \quad (BDE_{NH}) \qquad (2)$$

Applying doublet (**6** and **3a**) and OSS (**10**) ground state configurations, respectively, the resulting N−H BDE_{NH2} (eq 1) and BDE_{NH} (eq 2) values (see Supporting Information for details) confirm the experimentally estimated limits from reactions A−D. As a result, disproportionation of the imido species to the amide and nitride is exothermic by $\Delta H_{Diss} \cong -24$ kcal mol^{-1} ($\Delta G_{Diss} \cong -22$ kcal mol^{-1}). Kinetic barriers for bimolecular HAT were also calculated using the PMe_2-truncated models $\mathbf{6}^{Me}$, $\mathbf{3a}^{Me}$, and $\mathbf{10}^{Me}$. Low transition state barriers at both the triplet ($\Delta G^{\ddagger}$ = +8.4 kcal mol^{-1}) and the open-shell singlet ($\Delta G^{\ddagger}$ = +12.9 kcal mol^{-1}) potential energy surfaces (see Supporting Information) were obtained. These results are in line with reaction E and the transient nature of proposed intermediate **10**.

We previously reported that N−N coupling of iridium(IV) nitrido species **3a** to **4a** is exclusively observed, even in the presence of excess HAT reagent 1,4-cyclohexadiene.[31] Therefore, the hypothetical HAT reaction with 1,4-cyclohexadiene was also evaluated computationally. Overall, double HAT of 1,4-cyclohexadiene with nitride $\mathbf{3a}^{Me}$ to amide $\mathbf{6}^{Me}$ and benzene is strongly exergonic by −63.7 kcal mol^{-1} (Scheme 16). However, imido complex $\mathbf{10}^{Me}$ and the cyclohexadienyl radical define unfavorable intermediates, and the slightly endergonic first HAT reaction (ΔG^0 = +1.5 kcal mol^{-1}) is accompanied by a large kinetic barrier ($\Delta G^{\ddagger}$ = 24.4 kcal mol^{-1}). In comparison, bimolecular nitride coupling of $\mathbf{3a}^{Me}$ to $\mathbf{4a}^{Me}$, which is strongly downhill by ΔG^0 = −108.0 kcal mol^{-1} (−54.0 kcal mol^{-1} p. $\mathbf{3a}^{Me}$), was computed to proceed via a much lower transition state barrier ($\Delta G^{\ddagger}$ = 13.7 kcal mol^{-1}).[31]

In contrast to the first hydrogen transfer, the second HAT step from the cyclohexadienyl radical to $\mathbf{10}^{Me}$ (Scheme 16) exhibits a much smaller barrier ($\Delta G^{\ddagger}$ = 9.2 kcal mol^{-1}), as expected qualitatively from the large driving force ($\Delta\Delta G^0$ = −65.2 kcal mol^{-1}). Similarly, HAT of the reactive imido complex with parent cyclohexadiene is exergonic ($\Delta\Delta G^0$ = −21.2 kcal mol^{-1}) with a moderate barrier ($\Delta G^{\ddagger}$ = +16.7 kcal mol^{-1}).

DOI: 10.1021/acs.inorgchem.5b00829
Inorg. Chem. 2015, 54, 9290−9302

Scheme 16. DFT Computed Free Energies ($\Delta G_{298K}{}^{0}$) and Kinetic Barriers ($\Delta G_{298K}{}^{\ddagger}$) for HAT Reactions from 1,4-Cyclohexadiene to $3a^{Me}$ and 10^{Me} and for Nitride Coupling of $3a^{Me}$, Respectively (Energies in kcal mol^{-1})

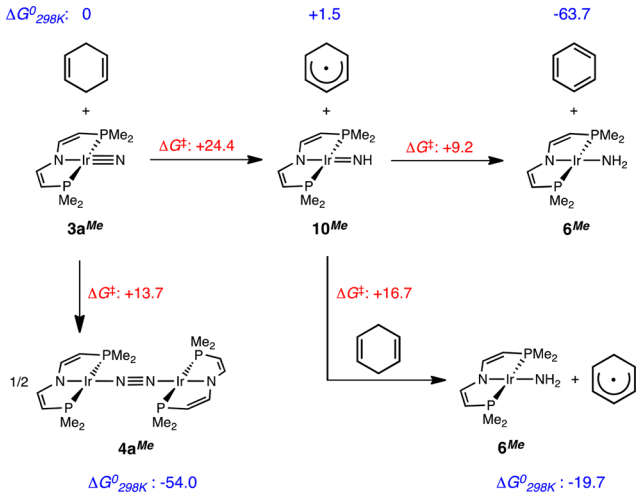

DISCUSSION

We recently presented square-planar complexes in a wide range of formal oxidation states, such as $[Ir^{I}Cl(PNP)]^{-}$, $[Ir^{II}Cl(PNP)]$ (**5**), $[Ir^{III}Cl(PNP)]^{+}$ (**9**), $[Ir^{IV}N(PNP)]$ (**3a**), and $[Ir^{V}N(PNP)]^{+}$ (**1**).[32,44,51] In the present study, parent iridium(II) amide and ammine complexes **6** and **7** and iridium(III) amide complex **8** were isolated and fully characterized. These compounds represent intermediates within a synthetic cycle of ammonia oxidation to dinitrogen (Scheme 17).

Scheme 17. Synthetic Cycle of NH_3 Oxidation with the Ir(PNP) Platform (Reaction with Dashed Arrow Not Demonstrated in This Work)

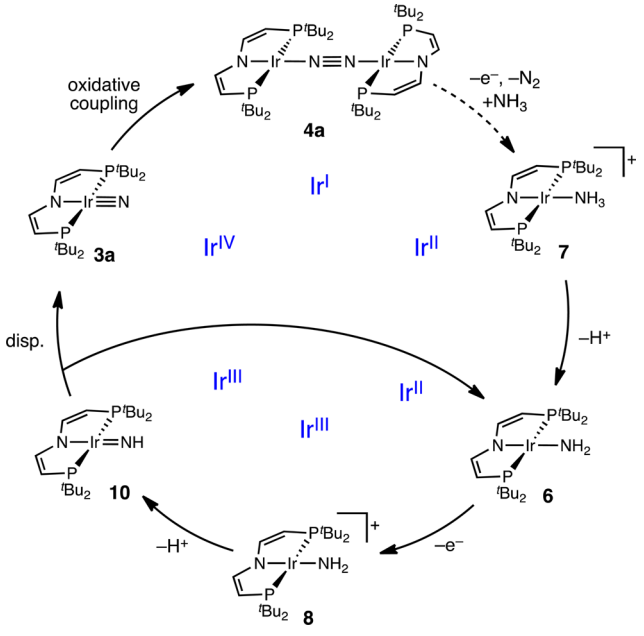

Once again the isolobal relationship with octahedral group 8 complexes shall be stressed (Figure 6). This analogy emphasizes the conservation of a square-planar geometry around iridium, which relies on steric shielding through the bulky

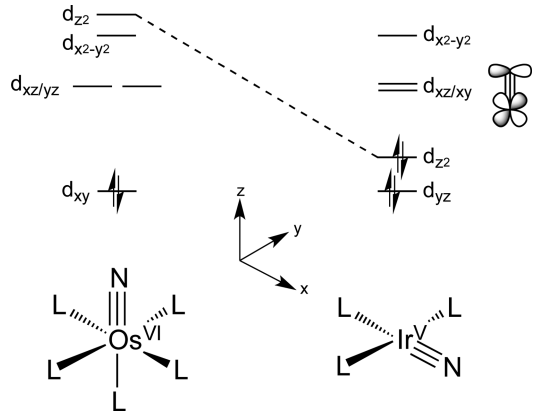

Figure 6. Schematic d-orbital splitting diagrams illustrating the isolobal relationship of octahedral d^2 (Os^{VI}) and square-planar d^4 (Ir^{V}) nitrido complexes.

pincer ligand. In several respects, the square-planar iridium compounds resemble the reactivity of octahedral polypyridyl Os−NH_x complexes, which undergo a fascinating redox chemistry.[55] For example, the octahedral nitrides $[Os^{VI}(N)Cl_2(L)]^{+}$ (L = tris(1-pyrazolyl)methane (tpm); 2,2′:6,2″-terpyridine (tpy); isolobal with **1**) also undergo nitride coupling to the N_2 bridged Os^{III}/Os^{III} complexes upon one-electron reduction.[35e] Furthermore, the reversible interconversion of the Os^{VI} nitrides and Os^{III} ammine complexes, $[Os^{III}(NH_3)Cl_2(L)]^{+}$ (isolobal with **7**), was studied electrochemically in depth by Meyer and co-workers.[56] The transient osmium(V) nitride stage (isolobal with **3a**) was not directly observed electrochemically. However, it could be trapped upon use of an anionic tridentate ligand: $[(Tp)Os^{VI}(N)Cl_2]$ (Tp = hydridotris(pyrazol-1-yl)borate) reduction in strongly acidic solution afforded the isolation of parent Os^{V} imide $[(Tp)Os^{V}(NH)Cl_2]$.[57] In neutral aqueous solution, the electrochemical studies of the tpy and tpm systems show that the redox couple $Os^{V}(N)/Os^{IV}(NH_2)$ (isolobal with **8**) provides a kinetic bottleneck for ammine/nitride interconversion as it is associated with multiple proton transfer steps. The parent $Os^{IV}(NH)$ imide (isolobal with **10**) is a likely intermediate, but the exact proton compositions of electrochemically detected $Os^{IV}(NH_x)$ species remain unclear. Notably, the spectroscopic identification of intermediates on the Os^{V} and Os^{IV} redox stages is hampered due to their inherent tendency to disproportionate, e.g.[56,55]

$$3[TpOs^{V}(NH)Cl_2] \rightarrow 2[TpOs^{VI}(N)Cl_2] + [TpOs^{III}(NH_3)Cl_2] \quad (3)$$

$$3[Os^{IV}(NH_2)Cl_2(tpy)]^{2+} \rightarrow [Os^{VI}(N)Cl_2(tpy)] + 2[Os^{III}(NH_3)Cl_2(tpy)] \quad (4)$$

In the current work, we particularly focused on the putative, parent Ir^{III} imido intermediate **10**, owing to its possible relation to reactive imides that show nitrene transfer reactivity. Well characterized terminal, parent TM imides are not very frequent and for the most part limited to high-valent, early TMs (group 4−6).[42b,58] Notably, Basolo and co-workers postulated a transient, electrophilic iridium parent imido, $[Ir(NH)(NH_3)_5]^{3+}$, as an intermediate in the decomposition of the respective azide $[IrN_3(NH_3)_5]^{2+}$, under acidic conditions.[59] All efforts to isolate **10** upon deprotonation of **8**, HAA from **6**, or

DOI: 10.1021/acs.inorgchem.5b00829
Inorg. Chem. 2015, 54, 9290−9302

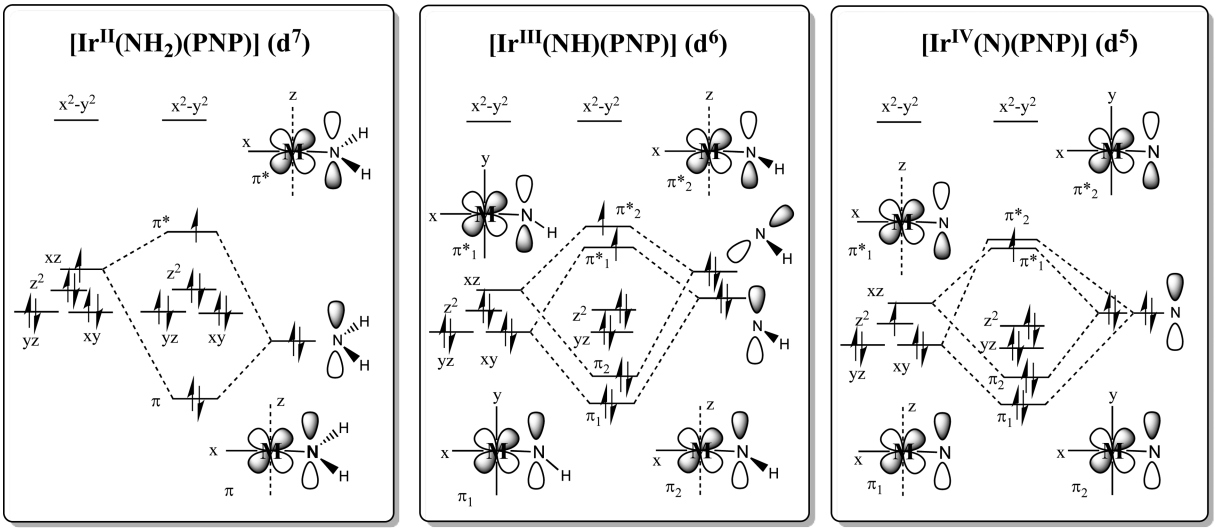

Figure 7. Qualitative representation of the frontier orbital interactions within amide **6**, imide **10** (only triplet state is shown), and nitride **3a**.

hydrogen transfer to **3a** were unsuccessful. NMR monitoring of the first reaction suggests detection of diamagnetic **10** as a reactive intermediate at low temperatures. However, at room temperature, spectroscopic and electrochemical examination indicates disproportionation of **10** into **3a** and **6** (Scheme 17), which is succeeded by nitride coupling, again in analogy with the osmium system. The HAT experiments of the nitride **3a** and amide **6** with TEMPO/TEMPO-H and TBP/TBP-H, respectively, confirm the disproportionation (reaction E) and allow for an estimate of boundaries for the amide and imide N−H BDEs. These are in agreement with the DFT computed values of 95 kcal mol^{-1} (**6**) and 71 kcal mol^{-1} (**10**), respectively. Also, a relatively high barrier for HAT from model substrate 1,4-cyclohexadiene to iridium(IV) nitride **3a** was computed, which cannot compete with decay upon bimolecular nitride coupling. Hence, the absence of reactivity of nitride **3a** with hydrocarbon HAT reagents and high selectivity toward nitride coupling is attributed to both thermodynamics and kinetics. Imide **10** seems more suitable for radical C−H activation due to the formation of a strong N−H bond. However, this reaction will compete with imide disproportionation proceeding at low barriers ($\mathbf{10^{Me}}$: $\Delta G^{\ddagger}$ = +8.4 kcal mol^{-1}). Hence, clean C−H activation and NH-group transfer will be a difficult task for kinetic reasons.

These results can be rationalized with qualitative frontier MO considerations within the IrNH$_x$ redox series. The SOMO of the amido species **6** (Figure 7 left, π^*) is mainly metal centered (d_{xz}) with some Ir−N$_{amido}$ π-antibonding contribution. HAA and formation of imide **10** results in overlap of another nitrogen lone-pair with an Ir d orbital (d_{xy}), which is a subject of the Ir−N−H bond angle. The high degree of covalency within the two Ir−N orbital interactions with π symmetry produces two high lying orbitals (Figure 7 center, π_1* and π_2*), which are occupied with overall two electrons in the three accessible states (CSS, OSS, T). In comparison, the two Ir−N MOs with π^*-character in nitride **3a** (Figure 7 right, π_1* and π_2*) are only occupied with overall one electron. Hence, disproportionation of the Ir^{III}-imide by intermolecular HAT to the Ir^{II}-amide and Ir^{IV}-nitride results in stabilization upon both reduction of covalent Ir−N interactions (**6**) and reduction of the population of antibonding orbitals (**3a**), respectively.

Our results indicate that, for such square-planar group 9 M^{II}−NH$_2$/M^{III}=NH/M^{IV}≡N compounds, the d^6 imido species should be best suited for E−H activation via HAT. The same arguments should qualitatively also apply to isolobal platforms. However, prevention of parent imide disproportionation will be a challenging task, and application of primary amines as a nitrogen source is advised.

EXPERIMENTAL SECTION

All experiments were carried out using Schlenk and glovebox (argon atmosphere) techniques. All solvents were dried by passing through columns packed with activated alumina. Deuterated solvents were obtained from Euriso-Top GmbH, dried over Na/K (d_6-benzene, d_8-THF, and d_8-toluene) or CaH$_2$ (CD$_2$Cl$_2$), respectively, distilled by trap-to-trap transfer *in vacuo* and degassed by three freeze−pump−thaw cycles. NaNH$_2$ (Acros), AgPF$_6$ (ABCR), AgSbF$_6$ (ABCR), TEMPO (Acros) and TBP−H (Acros) were used as purchased. **3a**,[44] [Ir(N$_3$)(PNP)],[31] TEMPO−H,[60] [H(Et$_2$O)$_2$][BAr$_4^F$],[61] and TBP[62] were prepared according to published procedures. Irradiation was carried out using a LOT-Quantum design 150 W xenon short-arc lamp. Elemental analyses were obtained from the analytical laboratories at the Georg-August University on an Elementar Vario EL 3. NMR spectra were recorded on Bruker Avance III 300 or 400 MHz spectrometers and were calibrated to the residual solvent proton resonance (d_6-benzene: δ_H = 7.16 ppm, δ_C = 128.39 ppm; d_8-THF: δ_H = 3.58 ppm, δ_C = 67.2 ppm; d_8-toluene: δ_H = 2.09 ppm, δ_C = 20.4 ppm; CD$_2$Cl$_2$: δ_H = 5.32 ppm, δ_C = 53.84 ppm). ^{31}P chemical shifts are reported relative to external phosphoric acid. Signal multiplicities are abbreviated as s (singlet), d (dublet), t (triplet), q (quartet), m (multiplet), and br (broad). Magnetic moments were determined in benzene at room temperature by Evans' method as modified by Sur and corrected for diamagnetic contribution.[63]

[Ir(NH$_2$)(PNP)] (6). 15-Crown-5 (43 μL; 0.21 mmol; 1 equiv) is added to a mixture of **5** (126 mg; 0.21 mmol; 1 equiv) and NaNH$_2$ (90.0 mg; 2.15 mmol; 10 equiv) in THF (10 mL, freshly dried over Na/K) and stirred for 3.5 h. All volatiles are removed in vacuo, the residue is extracted with benzene (3 × 7 mL), and the solvent is evaporated to dryness. After extraction of the crude product with pentanes (8 × 5 mL) and filtration over Celite, the solvent is removed, and the product is lyophilized overnight out of benzene (15 mL). **6** is obtained as green crude product and purified by sublimation (yield: 55%). Anal. Calcd for C$_{20}$H$_{42}$N$_2$P$_2$Ir (564.73): C, 42.54; H, 7.50; N, 4.96. Found: C, 42.87; H, 7.41; N, 4.73. NMR (d_6-benzene): ^{1}H (300 MHz, 20 °C): δ 5.96 (br, CH$_3$), −53.88 (br), −73.11 (br). $\mu_{eff}^{297\ K}$ = 1.82 μ_B.

[Ir(NH$_3$)(PNP)][B(Ar^F)$_4$] (7). [H(OEt$_2$)$_2$][B(Ar^F)$_4$] (47.0 mg; 65.9 μmol; 1.24 equiv) and **6** (30.0 mg; 53.1 μmol; 1 equiv) are dissolved in d_8-THF (0.5 mL) and shaken for 5 min. The product is precipitated with pentanes (2 mL), collected by filtration and washed

DOI: 10.1021/acs.inorgchem.5b00829
Inorg. Chem. 2015, 54, 9290−9302

with pentanes (3 × 2 mL). **7** is isolated as a blue solid (30.9 mg; 21.6 μmol; 41%). Anal. Calcd for $C_{52}H_{55}BF_{24}N_2P_2Ir$ (1428.96): C, 43.71; H, 3.88; N, 1.96. Found: C, 43.91; H, 3.82; N, 1.61. NMR (d_8-THF, 20 °C): δ 38.3 (br, 2H), 13.5 (br, 36H, CH_3), 7.77 (s, 8H, *o*-$C_6H_3(CF_3)_2$), 7.52 (s, 4H, *p*-$C_6H_3(CF_3)_2$).

[Ir(NH$_2$)(PNP)]PF$_6$ (8). A mixture of **6** (50.0 mg; 88.5 μmol) and $AgPF_6$ (22.4 mg; 88.5 μmol) is dissolved in THF (20 mL) and stirred for 5 min. After removal of the solvent, the residue is washed with benzene (4 × 5 mL), and the crude product is extracted with THF (8 × 5 mL). The solution is concentrated, layered with pentanes (40 mL), and crystallized at −32 °C for 16 h. Deep purple crystalline **8** is filtered off, washed with pentanes (4 × 5 mL), and dried in vacuo (50.3 mg; 63.0 μmol; 71%). Anal. Calcd for $C_{20}H_{42}N_2F_6P_2Ir$ (709.70): C, 33.85; H, 5.97; N, 3.95. Found: C, 33.99; H, 5.78; N, 3.48. NMR (CD_2Cl_2, 20 °C), ^{1}H NMR: 11.35 (br, 2H, NH_2), 6.35 (ABXX′B′A′, $N = |^2J_{HP} + {}^4J_{HP}| = 4.7$ Hz, $^3J_{HH} = 6.3$ Hz, 2H, NCHC*H*P), 6.11 (ABXX′B′A′, $N = |^3J_{HP} + {}^5J_{HP}| = 17.7$ Hz, $^3J_{HH} = 6.3$ Hz, 2H, NC*H*CHP), 1.66 ($A_{18}XX'A'_{18}$, $N = |^3J_{HP} + {}^5J_{HP}| = 7.5$ Hz, 36H, CH_3). ^{13}C (75.47 MHz): δ 169.6 (AXX′A′, $N = |^2J_{CP} + {}^3J_{CP}| = 6.0$ Hz, NCHCHP), 121.2 (AXX′A′, $N = |^1J_{CP} + {}^3J_{CP}| = 18.4$ Hz, NCHCHP), 36.5 ($A_2XX'A'_2$, $N = |^1J_{CP} + {}^3J_{CP}| = 11.7$ Hz, $PCCH_3$), 31.4 ($A_6XX'A'_6$, $N = |^2J_{CP} + {}^4J_{CP}| = 2.7$ Hz, $PCCH_3$). ^{31}P (121.49 MHz): δ 48.2 (s, *Pt*Bu_{23}), −145 (hept, $^1J_{PF} = 710.5$ Hz, PF_6).

■ ASSOCIATED CONTENT

Supporting Information

Additional experimental procedures, spectroscopic, and computational data in pdf and crystallographic data in cif format. The Supporting Information is available free of charge on the ACS Publications website at DOI: 10.1021/acs.inorgchem.5b00829.

■ AUTHOR INFORMATION

Corresponding Authors

*E-mail: b.debruin@uva.nl.

*E-mail: sven.schneider@chemie.uni-goettingen.de.

Notes

The authors declare no competing financial interest.

■ ACKNOWLEDGMENTS

Financial support by the DFG (Emmy-Noether program grant SCHN950/2-1, S.S.), the ERC (grant number 202886, B.d.B.), NWO−CW (VICI grant number 016.122.613, B.d.B.), and COST action CM1205 (CARISMA) is gratefully acknowledged.

■ REFERENCES

(1) (a) Eikey, R. A.; Abu-Omar, M. M. *Coord. Chem. Rev.* **2003**, *243*, 83. (b) Berry, J. F. *Comments Inorg. Chem.* **2009**, *30*, 28. (c) Saouma, C. T.; Peters, J. C. *Coord. Chem. Rev.* **2011**, *255*, 920. (d) Hohenberger, J.; Ray, K.; Meyer, K. *Nature Commun.* **2012**, *3*, 720. (e) Olivos Suarez, A. I.; Lyaskovskyy, V.; Reek, J. N. H.; van der Vlugt, J. I.; de Bruin, B. *Angew. Chem., Int. Ed.* **2013**, *52*, 12510. (f) Smith, J. *Prog. Inorg. Chem.* **2014**, *58*, 417. (g) Kornecki, K. P.; Berry, J. F.; Powers, D. C.; Ritter, T. *Prog. Inorg. Chem.* **2014**, *58*, 225.

(2) (a) Liang, J.-L.; Yuan, S.-X.; Huang, J.-S.; Che, C.-M. *J. Org. Chem.* **2004**, *69*, 3610. (b) Davies, H. M. L. *Angew. Chem., Int. Ed.* **2006**, *45*, 6422. (c) Davies, H. M. L.; Manning, J. R. *Nature* **2008**, *451*, 417. (d) Fiori, K. W.; Espino, C. G.; Brodsky, B. H.; Du Bois, J. *Tetrahedron* **2009**, *65*, 3042. (e) Berry, J. F. *Dalton Trans.* **2012**, *41*, 700. (f) Roizen, J. L.; Harvey, M. E.; Du Bois, J. *Acc. Chem. Res.* **2012**, *45*, 911. (g) Dequirez, G.; Pons, V.; Dauban, P. *Angew. Chem., Int. Ed.* **2012**, *51*, 7384. (h) Jeffrey, J. L.; Sarpong, R. *Chem. Sci.* **2013**, *4*, 4092.

(3) Mann, J. B.; Meek, T. L.; Knight, E. T.; Capitani, J. F.; Allen, L. C. *J. Am. Chem. Soc.* **2000**, *122*, 5132.

(4) Harrison, J. F. *Chem. Rev.* **2000**, *100*, 679.

(5) Perry, R. H.; Cahill, T. J., III; Roizen, J. L.; Du Bois, J.; Zare, R. N. *Proc. Nat. Acad. Sci.* **2012**, *109*, 18295.

(6) Wiese, S.; Badiei, Y. M.; Gephart, R. T.; Mossin, S.; Varonka, M. S.; Melzer, M. M.; Meyer, K.; Cundari, T. R.; Warren, T. H. *Angew. Chem., Int. Ed.* **2010**, *49*, 8850.

(7) Kornecki, K. P.; Berry, J. F. *Chem.—Eur. J.* **2011**, *17*, 5827.

(8) (a) Rees, N. V.; Compton, R. G. *Energy Environ. Sci.* **2011**, *4*, 1255. (b) Schüth, F.; Palkovits, R.; Schlögl, R.; Su, D. S. *Energy Environ. Sci.* **2012**, *5*, 6278.

(9) (a) Schrock, R. R. *Angew. Chem., Int. Ed.* **2008**, *47*, 5512. (b) Licht, S.; Cui, B.; Wang, B.; Li, F.-F.; Lau, J.; Liu, S. *Science* **2014**, *345*, 637. (c) Van der Ham, C. J. M.; Koper, M. T. M.; Hetterscheid, D. G. H. *Chem. Soc. Rev.* **2014**, *43*, 5183.

(10) Throughout this paper, bond dissociation enthalpies, as defined by reaction enthalpies (Δ_rH_{A-B}) of bond cleavage (AB → A + B), are abbreviated as BDE. These values are not identical with spectroscopic bond dissociation energies (D_0), that are also often abbreviated BDE (ref 11).

(11) Blanksby, S. J.; Ellison, G. B. *Acc. Chem. Res.* **2003**, *36*, 255.

(12) Bordwell, F. G.; Drucker, G. E.; Fried, H. E. *J. Org. Chem.* **1981**, *46*, 632.

(13) (a) Hillhouse, G. L.; Bercaw, J. E. *J. Am. Chem. Soc.* **1984**, *106*, 5472. (b) Roesky, H. W.; Bai, Y.; Noltemeyer, M. *Angew. Chem., Int. Ed. Engl.* **1989**, *28*, 754. (c) Holl, M. M. B.; Kersting, M.; Pendley, B. D.; Wolczanski, T. T. *Inorg. Chem.* **1990**, *29*, 1518. (d) Nakajima, Y.; Kameo, H.; Suzuki, H. *Angew. Chem., Int. Ed.* **2006**, *45*, 950. (e) Peng, Y.; Ellis, B. D.; Wang, X.; Power, P. P. *J. Am. Chem. Soc.* **2008**, *130*, 12268. (f) Ni, C.; Lei, H.; Power, P. P. *Organometallics* **2010**, *29*, 1988. (g) Shima, T.; Hou, Z. *Dalton Trans.* **2010**, *39*, 6858. (h) Khaskin, E.; Iron, M. A.; Shimon, L. J. W.; Zhang, J.; Milstein, D. *J. Am. Chem. Soc.* **2010**, *132*, 8542. (i) Gutsulyak, D. V.; Piers, W. E.; Borau-Garcia, J.; Parvez, M. *J. Am. Chem. Soc.* **2013**, *135*, 11776. (j) Chang, Y.-H.; Nakajima, Y.; Tanaka, H.; Yoshizawa, K.; Ozawa, F. *J. Am. Chem. Soc.* **2013**, *135*, 11791.

(14) (a) Casalnuovo, A. L.; Calabrese, J. C.; Milstein, D. *Inorg. Chem.* **1987**, *26*, 973. (b) Zhao, J.; Goldman, A. S.; Hartwig, J. F. *Science* **2005**, *307*, 1080.

(15) Fafard, C. M.; Adhikari, d.; Foxman, B. M.; Mindiola, D. J.; Ozerov, O. V. *J. Am. Chem. Soc.* **2007**, *129*, 10318.

(16) (a) Glueck, D. S.; Hollander, F. J.; Bergman, R. G. *J. Am. Chem. Soc.* **1989**, *111*, 2719. (b) Glueck, D. S.; Wu, J. X.; Hollander, F. J.; Bergman, R. G. *J. Am. Chem. Soc.* **1991**, *113*, 2041. (c) Jenkins, D. M.; Betley, T. A.; Peters, J. C. *J. Am. Chem. Soc.* **2002**, *124*, 11238. (d) Hu, X. L.; Meyer, K. *J. Am. Chem. Soc.* **2004**, *126*, 16322. (e) Shay, D. T.; Yap, G. P. A.; Zakharov, L. N.; Rheingold, A. L.; Theopold, K. H. *Angew. Chem., Int. Ed.* **2005**, *44*, 1508. (f) Shay, D. T.; Yap, G. P. A.; Zakharov, L. N.; Rheingold, A. L.; Theopold, K. H. *Angew. Chem., Int. Ed.* **2006**, *45*, 7870. (g) Cowley, R. E.; Bontchev, R. P.; Sorrell, J.; Sarracino, O.; Feng, Y.; Wang, H.; Smith, J. M. *J. Am. Chem. Soc.* **2007**, *129*, 2424. (h) Geer, A. M.; Tejel, C.; López, J. A.; Ciriano, M. A. *Angew. Chem., Int. Ed.* **2014**, *53*, 5614.

(17) King, E. R.; Sazama, G. T.; Betley, T. A. *J. Am. Chem. Soc.* **2012**, *134*, 17858.

(18) (a) Harden, J. D.; Ruppel, J. V.; Gao, G.-Y.; Zhang, X. P. *Chem. Commun.* **2007**, 4644. (b) Ruppel, J. V.; Kamble, R. M.; Zhang, X. P. *Org. Lett.* **2007**, *9*, 4889. (c) Lu, H.; Jiang, H.; Wojtas, L.; Zhang, X. P. *Angew. Chem., Int. Ed.* **2010**, *49*, 10192. (d) Lu, H.; Tao, J.; Jones, J. E.; Wojtas, L.; Zhang, X. P. *Org. Lett.* **2010**, *12*, 1248. (e) Lyaskovskyy, V.; Suarez, A. I. O.; Lu, H.; Jiang, H.; Zhang, X. P.; de Bruin, B. *J. Am. Chem. Soc.* **2011**, *133*, 12264. (f) Suarez, A. I. O.; Jiang, H.; Zhang, X. P.; de Bruin, B. *Dalton Trans.* **2011**, *40*, 5697. (g) Goswami, M.; Lyaskovskyy, V.; Domingos, S. R.; Buma, W. J.; Woutersen, S.; Troeppner, O.; Ivanović-Burmazović, I.; Lu, H.; Cui, X.; Zhang, X. P.; Reijerse, E. J.; DeBeer, S.; van Schooneveld, M. M.; Pfaff, F.; Ray, K.; de Bruin, B. *J. Am. Chem. Soc.* DOI: 10.1021/jacs.5b01197.

(19) (a) Mindiola, D. J.; Hillhouse, G. L. *J. Am. Chem. Soc.* **2001**, *123*, 4623. (b) Waterman, R.; Hillhouse, G. L. *J. Am. Chem. Soc.* **2008**, *130*, 12628. (c) Ilic, V. M.; Hillhouse, G. L. *J. Am. Chem. Soc.* **2010**, *132*, 15148.

DOI: 10.1021/acs.inorgchem.5b00829
Inorg. Chem. 2015, 54, 9290−9302

(20) (a) Mindiola, D. J.; Hillhouse, G. L. *Chem. Commun.* **2002**, 1840. (b) Mindiola, D. J.; Waterman, R.; Iluc, V. M.; Cundari, T. R.; Hillhouse, G. L. *Inorg. Chem.* **2014**, *53*, 13227.
(21) Iluc, V. M.; Miller, A. J. M.; Anderson, J. S.; Monreal, M. J.; Mehn, M. P.; Hillhouse, G. L. *J. Am. Chem. Soc.* **2011**, *133*, 13055.
(22) Harrold, N. D.; Hillhouse, G. L. *Chem. Sci.* **2013**, *4*, 4011.
(23) (a) Ge, Y.-W.; Ye, Y.; Sharp, P. R. *J. Am. Chem. Soc.* **1994**, *116*, 8384. (b) Bai, G.; Stephan, D. W. *Angew. Chem., Int. Ed.* **2007**, *46*, 1856.
(24) Kondo, O.; Benson, S. W. *Int. J. Chem. Kinet.* **1984**, *16*, 949.
(25) Kogut, E.; Wiencko, H. L.; Zhang, L.; Cordeau, D. E.; Warren, T. H. *J. Am. Chem. Soc.* **2005**, *127*, 11248.
(26) Wiese, S.; McAfee, J. L.; Pahls, D. R.; McMullin, C. L.; Cundari, T. R.; Warren, T. H. *J. Am. Chem. Soc.* **2012**, *134*, 10114.
(27) Badiei, Y. M.; Dinescu, A.; Dai, X.; Palomino, R. M.; Heinemann, F. W.; Cundari, T. R.; Warren, T. H. *Angew. Chem., Int. Ed.* **2008**, *47*, 9961.
(28) Kundu, S.; Miceli, E.; Farquhar, E. R.; Pfaff, F. F.; Kuhlmann, U.; Hildebrandt, P.; Braun, B.; Greco, C.; Ray, K. *J. Am. Chem. Soc.* **2012**, *134*, 14710.
(29) (a) Schöffel, J.; Rogachev, A. Y.; DeBeer George, S.; Burger, P. *Angew. Chem., Int. Ed.* **2009**, *48*, 4734. (b) Sieh, D.; Schöffel, J.; Burger, P. *Dalton Trans.* **2011**, *40*, 9512.
(30) Sieh, D.; Burger, P. *J. Am. Chem. Soc.* **2013**, *135*, 3971.
(31) Scheibel, M. G.; Askevold, B.; Heinemann, F. W.; Reijerse, E. J.; de Bruin, B.; Schneider, S. *Nat. Chem.* **2012**, *4*, 552.
(32) Scheibel, M. G.; Wu, Y.; Stückl, a C.; Krause, L.; Carl, E.; Stalke, D.; de Bruin, B.; Schneider, S. *J. Am. Chem. Soc.* **2013**, *5*, 17719.
(33) Zolnhofer, E. M.; Käß, M.; Khusniyarov, M. M.; Heinemann, F. W.; Maron, L.; van Gastel, M.; Bill, E.; Meyer, K. *J. Am. Chem. Soc.* **2014**, *136*, 15072.
(34) Gloaguen, Y.; Rebreyend, C.; Lutz, M.; Kumar, P.; Huber, M.; van der Vlugt, J. I.; Schneider, S.; de Bruin, B. *Angew. Chem., Int. Ed.* **2014**, *53*, 6814.
(35) (a) Kane-Maguire, L. A. P.; Sheridan, P. S.; Basolo, F.; Pearson, R. G. *J. Am. Chem. Soc.* **1970**, *92*, 5865. (b) Buhr, J. D.; Taube, H. *Inorg. Chem.* **1979**, *18*, 2208. (c) Che, C.-M.; Lam, H.-W.; Tong, W.-F.; Lai, T.-F.; Lau, T.-C. *J. Chem. Soc. Chem. Commun.* **1989**, 1883. (d) Ware, D. C.; Taube, H. *Inorg. Chem.* **1991**, *30*, 4605. (e) Demandis, K. D.; Meyer, T. J.; White, P. S. *Inorg. Chem.* **1997**, *36*, 5678. (f) Krahe, O.; Bill, E.; Neese, F. *Angew. Chem., Int. Ed.* **2014**, 8727.
(36) Sellmann, D. *Angew. Chem., Int. Ed.* **1974**, *13*, 639.
(37) Sanner, R. D.; Manriquez, J. M.; Marsh, R. E.; Bercaw, J. E. *J. Am. Chem. Soc.* **1976**, *98*, 8351.
(38) The notation $\{M-N-N-M\}^n$ here gives the number of electrons n in the π-MO manifold derived from linear combination of the four M(d) and four N(p) orbitals with π symmetry. It should not be confused with the Enemark–Feltham notation for nitrosyl complexes or the analogous notation for terminal nitrides proposed by Wieghardt, which counts all metal d electrons: Bendix, J.; Meyer, K.; Weyhermüller, T.; Bill, E.; Metzler-Nolte, N.; Wieghardt, K. *Inorg. Chem.* **1998**, *37*, 1767.
(39) Laplaza, C. E.; Johnson, M. J. A.; Peters, J. C.; Odom, A. L.; Kim, E.; Cummins, C. C.; George, G. N.; Pickering, I. J. *J. Am. Chem. Soc.* **1996**, *118*, 8623.
(40) Examples: (a) Laplaza, C. E.; Cummins, C. C. *Science* **1995**, *268*, 861. (b) Klopsch, I.; Finger, M.; Würtele, C.; Milde, B.; Werz, D. B.; Schneider, S. *J. Am. Chem. Soc.* **2014**, *136*, 6881. (c) Miyazaki, T.; Tanaka, H.; Tanabe, Y.; Yuki, M.; Nakajima, K.; Yoshizawa, K.; Nishibayashi, Y. *Angew. Chem., Int. Ed.* **2014**, *53*, 11488.
(41) (a) Betley, T. A.; Peters, J. C. *J. Am. Chem. Soc.* **2004**, *126*, 6252. (b) Hendrich, M. P.; Gunderson, W.; Behan, R. K.; Green, M. T.; Mehn, M. P.; Betley, T. A.; Lu, C. C.; Peters, J. C. *Proc. Nat. Acad. Sci. U.S.A.* **2006**, *103*, 17107.
(42) (a) Thomson, R. K.; Thibault, C.; Scott, B. L.; Morris, D. E.; Batista, E. R.; Kiplinger, J. L. *Nat. Chem.* **2011**, *2*, 723. (b) Tran, B. L.; Washington, M. P.; Henckel, D. A.; Gao, X.; Park, H.; Pink, M.; Mindiola, D. J. *Chem. Commun.* **2012**, *48*, 1529. (c) King, D. M.; Tuna, F.; McInnes, E. J. L.; McMaster, J.; Lewis, W.; Blake, A. J.; Liddle, S. T. *Nat. Chem.* **2013**, *5*, 482.
(43) Atienza, C. C. H.; Bowman, A. C.; Lobkovsky, E.; Chirik, P. J. *J. Am. Chem. Soc.* **2010**, *132*, 16343.
(44) Meiners, J.; Scheibel, M. G.; Lemée-Cailleau, M.-H.; Mason, S. A.; Boeddinghaus, M. B.; Fässler, T. F.; Herdtweck, E.; Khusniyarov, M. M.; Schneider, S. *Angew. Chemie Int. Ed.* **2011**, *50*, 8184.
(45) Büttner, T.; Geier, J.; Frison, G.; Harmer, J.; Calle, C.; Schweiger, A.; Schönberg, H.; Grützmacher, H. *Science* **2005**, *307*, 235.
(46) The diamagnetic, square-planar chloro complex [Ir(Cl){$C(CH_2CH_2P^tBu_2)$}] is isoelectronic with **8**/**9**. However, oxidation state assignment as being an iridium(I) carbene (Fischer type) or iridium(III) alkylidene (Schrock type) complex is not straightforward: Empsall, H. D.; Hyde, E. M.; Markham, R.; McDonald, W. S.; Norton, M. C.; Shaw, B. L.; Weeks, B. *J. Chem. Soc., Chem. Commun.* **1977**, 589.
(47) Rais, D.; Bergman, R. G. *Chem.—Eur. J.* **2004**, *10*, 3970.
(48) (a) Askevold, B.; Khusniyarov, M. M.; Herdtweck, E.; Meyer, K.; Schneider, S. *Angew. Chem., Int. Ed.* **2010**, *49*, 7566. (b) Askevold, B.; Khusniyarov, M. M.; Kroener, W.; Gieb, K.; Müller, P.; Herdtweck, E.; Heinemann, F. W.; Diefenbach, M.; Holthausen, M. C.; Vieru, V.; Chibotaru, L. F.; Schneider, S. *Chem.—Eur. J.* **2015**, *21*, 579.
(49) ^{1}H NMR spectroscopic in situ assignment of the paramagnetic complexes **3a** and **6** are unequivocal and rely on comparison with the full set of signals obtained from original samples at the respective temperatures.
(50) Kanzelberger, M.; Zhang, X.; Emge, A. S.; Goldman, A. S.; Zhao, J.; Incarvito, C.; Hartwig, J. F. *J. Am. Chem. Soc.* **2003**, 13644.
(51) Kinauer, M.; Scheibel, M. G.; Abbenseth, J.; Heinemann, F. W.; Stollberg, P.; Würtele, C.; Schneider, S. *Dalton Trans.* **2014**, *43*, 4506.
(52) Electrochemical activity of $K[N(SiMe_3)_2]$ at these conditions in the examined potential window is excluded by the absence of CV features for pure $K[N(SiMe_3)_2]$ in THF between 0 and −3.5 V (Supporting Information Figure S8).
(53) Reactions B–E were monitored by ^{1}H NMR spectroscopy at −60 °C to prevent bimolecular nitride coupling of **3a** to **4a**. Therefore, BDE values are discussed, although BDFEs would be more appropriate (ref 53). Furthermore, integration of **3a** vs **6** (reaction E) had to be done at room temperature due to considerable *t*Bu-^{1}H-peak overlap at low *T*, adding some integration error from nitride coupling.
(54) Warren, J. J.; Tronic, T. A.; Mayer, J. M. *Chem. Rev.* **2010**, *110*, 6961.
(55) Meyer, T. J.; Huynh, M. H. V. *Inorg. Chem.* **2003**, *42*, 8140.
(56) (a) Pipes, D. W.; Bakir, M.; Vitols, S. E.; Hogdson, D. J.; Meyer, T. J. *J. Am. Chem. Soc.* **1990**, *112*, 5507. (b) Coia, G. M.; Demadis, K. D.; Meyer, T. J. *Inorg. Chem.* **2000**, *39*, 2212. (c) El-Samanody, E.-S.; Demadis, K. D.; Meyer, T. J.; White, P. S. *Inorg. Chem.* **2001**, *40*, 3677.
(57) Huynh, M. H. V.; White, P. S.; John, K. D.; Meyer, T. J. *Angew. Chem., Int. Ed.* **2001**, *40*, 4049.
(58) (a) Chatt, J.; Dilworth, J.; Richards, R. *Chem. Rev.* **1978**, *78*, 589. (b) Bevan, P. C.; Chatt, J.; Dilworth, J. R.; Henderson, R. A.; Leigh, G. J.; Peter, B.; Joseph, C. B.; Jonathan, C.; Richard, R. D. *J. Chem. Soc., Dalt. Trans.* **1982**, 821. (c) Schrock, R. R.; Glassman, T. E.; Vale, M. G. *J. Am. Chem. Soc.* **1991**, *7*, 725. (d) Parkin, G.; Asselt, A. Van; Leahy, D. J.; Whinnery, L.; Hua, N. G.; Quan, R. W.; Henling, L. M.; Schaefer, W. P.; Santarsiero, B. D.; Bercaw, J. E. *Inorg. Chem.* **1992**, *31*, 82. (e) Freundlich, J. S.; Schrock, R. R.; Cummins, C. C.; Davis, W. M.; Taciz, N. *J. Am. Chem. Soc.* **1994**, *116*, 1987. (f) Cummins, C. C.; Schrock, R. R.; Davis, W. M. *Inorg. Chem.* **1994**, *33*, 1448. (g) Opph, T. N. H.; Mckarns, P. J.; Yap, G. P. A.; Rheingold, A. L.; Winter, C. H. *Inorg. Chem.* **1996**, *2*, 5968. (h) Alias, Y.; Ibrahim, S. K.; Queiros, M. A.; Fonseca, A.; Talarmin, J.; Volant, F.; Pickett, C. J. *J. Chem. Soc. Dalt. Trans.* **1997**, 4807. (i) Yandulov, D. V.; Schrock, R. R. *J. Am. Chem. Soc.* **2002**, *124*, 6252. (j) Lutz, C. M.; Wilson, S. R.; Shapley, P. A. *Organometallics* **2005**, *24*, 3350. (k) Reithofer, M. R.; Schrock, R. R.; Mu, P. *J. Am. Chem. Soc.* **2010**, *132*, 8349. (l) Keane, A. J.; Zavalij, P. Y.; Sita, L. R. *J. Am. Chem. Soc.* **2013**, *135*, 9580. (m) Thompson, R.; Chen, C.-H.; Pink, M.; Wu, G.; Mindiola, D. J. *J. Am. Chem. Soc.* **2014**, *6917*, 15.

DOI: 10.1021/acs.inorgchem.5b00829
Inorg. Chem. 2015, 54, 9290–9302

(59) (a) Lane, B. C.; McDonal, J. W.; Basolo, F.; Pearson, R. G. *J. Am. Chem. Soc.* **1972**, *94*, 3786. (b) Gafney, H. D.; Reed, J. L.; Basolo, F. *J. Am. Chem. Soc.* **1973**, *95*, 7998.
(60) Giffin, N. A.; Makramalla, M.; Hendsbee, A. D.; Robertson, K. N.; Sherren, C.; Pye, C. C.; Masuda, J. D.; Clyburne, J. A. C. *Org. Biomol. Chem.* **2011**, *9*, 3672.
(61) Brookhart, M.; Grant, B.; Volpe, A. F., Jr. *Organometallics* **1992**, *11*, 3920.
(62) Manner, V. W.; Markle, T. F.; Freudenthal, J. H.; Roth, J. P.; Mayer, J. M. *Chem. Commun.* **2008**, *246*, 256.
(63) Sur, S. K. *J. Magn. Reson.* **1989**, *82*, 169.

DOI: 10.1021/acs.inorgchem.5b00829
Inorg. Chem. 2015, 54, 9290−9302